Nonlinear Analysis of Stability and Safety of Optimal Velocity Model Vehicle Groups on Ring Roads

Cristina Magnetti Gisolo, Maria Laura Delle Monache, Francesco Ferrante, Paolo Frasca

Nonlinear Analysis of Stability and Safety of Optimal Velocity Model Vehicle Groups on Ring Roads

Cristina Magnetti Gisolo, Maria Laura Delle Monache, Francesco Ferrante, and Paolo Frasca

***Abstract*—In this work, we study a group of N homogeneous vehicles travelling on a ring road by describing the collective vehicle dynamics via the so-called Optimal Velocity Model (OVM). We analyze the stability of the equilibrium motion regime in which all vehicles drive at the same speed and keep the same headway. First, stability is studied through linearization, thereby highlighting the roles of the model parameters. Next, we tackle the full nonlinear model and we determine ellipsoidal estimates of the equilibrium's region of attraction by defining and solving suitable Linear Matrix Inequalities (LMIs). Finally, safety aspects are discussed, incorporated in our LMI formulation as lower bounds of the inter-vehicle distances, and illustrated via simulations.**

I. Introduction

A. Background

Vehicular transportation is undergoing a major disruption, moving from vehicles in which the humans are completely responsible of all the driving tasks towards fully automated vehicles in which automation will be responsible of most (if not all) driving tasks. Furthermore, several experiments have shown that we can harvest the potential of automation towards traffic control and even a small number of automated vehicles can be effective in controlling traffic under specific circumstances. A seminal experiment featuring a group of vehicles on a ring road has been performed by Sugiyama et al. [1]. The ring road, in this case, is a representation of a road of infinite length that allows to observe in a controlled environment the phenomenon of the stop-and-go waves. More recent experiments in [2] show that stop-and-go waves produced by a group of human-driven vehicles on a ring road can be controlled by a small number of autonomous vehicles (AVs).

Traffic control through AVs aims to avoid large oscillations of the speed, sudden braking and acceleration, dissipate stop-and-go waves and make traffic flow more fluid. In particular, the objective of the control strategy is to make the group reach an equilibrium state, called uniform flow equilibrium, in which all vehicles travel at the same velocity and have the same headway. Despite the effectiveness of the use of AVs in traffic control, it is not clear by which mechanism their interconnection with human-driven vehicles stabilizes traffic: hence the need for advancing the study of the stability of traffic flows. In this perspective of control, in this work we analyze the stability of the uniform flow equilibrium in a specific mathematical description of traffic flow: the Optimal Velocity Model (OVM). Other models have also been proposed and studied in the literature; see, e.g., [3].

Several papers have looked at stability and string stability to explain the stability of multi-vehicle platoons; see, e.g., [4], [5]. In [6], the authors look at the linearized OVM and derive a linear string stability approach to the problem: this approach has been supplemented in [7] with specific string stability condition for ring roads. Indeed, most analytic studies on the topic of mixed traffic rely on the linearization of the nonlinear dynamics around the equilibrium flow [8], [9], [10]. Relevant exceptions include [11] and [12], where nonlinear approaches based on bifurcation theory are proposed to evaluate the role of delays and the impact of connected cruise control on connected vehicle system.

B. Contributions

In this paper, we try to overcome this simplification by moving from classical linear stability analysis to the study of the nonlinear dynamics and stability. Before the nonlinear analysis, we start by linearizing the nonlinear model around the uniform flow equilibrium and studying its stability through eigenvalue analysis. However, the linearization limits the study of stability to a local neighborhood of the equilibrium, preventing to derive any conclusion on the trajectories of the original nonlinear model when they are sufficiently far from the equilibrium point. For this reason, in the second part of this paper, we study stability by focusing on the nonlinear model and trying to identify its region of attraction through ellipsoidal estimates. By this method, we are able to determine a region of the state space from which the trajectories of the nonlinear model are guaranteed to converge to the equilibrium point. This method is computationally convenient because it is based on solving suitable Linear Matrix Inequalities (LMIs). Furthermore, safety constraints can be effectively incorporated in the analysis, thereby defining "safe" ellipsoidal regions of

C. Magnetti Gisolo was a student at Politecnico di Torino, Turin, Italy and a research intern at GIPSA-lab, Grenoble, France.

M. L. Delle Monache is with the Department of Civil and Environmental Engineering at the University of California, Berkeley; email: mldelle-monache@berkeley.edu. This work was partially done while she was with Univ. Grenoble Alpes, Inria, CNRS, Grenoble INP, GIPSA-lab, 38000 Grenoble, France.

Francesco Ferrante is with Department of Engineering, University of Perugia, Via G. Duranti, 67, 06125 Perugia, Italy, email: francesco.ferrante@unipg.it

P. Frasca are with Univ. Grenoble Alpes, CNRS, Inria, Grenoble INP, GIPSA-lab, 38000 Grenoble, France.

This work has been partly supported by ANR via grant HANDY, number ANR-18-CE40-0010.

attraction. The ability to compute safe invariant regions for the full nonlinear model is a key advantage of our approach for practical applications.

C. Outline

The article is organized as follows. In Section II we introduce the OVM model on a ring. Section III studies the stability of the model after linearization and how stability depends on the model parameters. Next, we move on to the nonlinear analysis of the model in Section IV by defining and computing regions of attraction. Section V builds on these methods and computes safety regions for the trajectories of the models to avoid collisions. Section VI concludes the article.

II. Optimal Velocity Model on a ring

The Optimal Velocity Model of N vehicles introduced by Bando et al. in [13] is described by:

$$\begin{cases} \dot{x}_i = v_i \\ \dot{v}_i = b\left[V_{opt}\left(x_{i+1} - x_i\right) - v_i\right] \end{cases}, \ \forall\ i = 1, \dots, N, \quad (1)$$

where b is a constant representing the sensitivity of the driver, x_i and v_i are the absolute position and velocity of the center of mass of the i-th vehicle and $\Delta x_i = x_{i+1} - x_i$ is the headway with respect to the preceding vehicle $i+1$. Suppose the N vehicles drive on a ring road of length L, then $N+1 = 1$. The optimal velocity function is:

$$V_{opt}(\Delta x_i) = V_{\max}\frac{\tanh\left(\Delta x_i - l_v - d_s\right) + \tanh\left(l_v + d_s\right)}{1 + \tanh\left(l_v + d_s\right)},$$

where $V_{\max}$ is the maximum speed, l_v is the vehicle length and d_s is the safe distance between vehicles i and $i+1$.
We are interested in a particular state, called speed equilibrium, in which the vehicles of model (1) drive with the same constant velocity v_*. Since the velocity function depends only on the headway, at the speed equilibrium also the vehicle distances are the same and equal to $\Delta x_* = L/N$. We refer to this particular state as uniform flow equilibrium, in which

$$\begin{aligned} x_{i+1} - x_i = \Delta x_* = \frac{L}{N} \coloneqq d \\ v_i = v_* = V_{opt}(d). \end{aligned} \quad (2)$$

Model (1) is rewritten in a new set of state variables such that the uniform flow equilibrium coincides with the origin of the new model. The new state variables are the relative velocities y_i of each couple of adjacent vehicles and the spacing errors z_i with respect to the distance $d = L/N$ at the uniform flow equilibrium. $z_i = x_{i+1} - x_i - d = \Delta x_i - d$, $y_i = v_{i+1} - v_i$. In these state variables, model (1) turns into

$$\begin{cases} \dot{z}_i = y_i \\ \dot{y}_i = b\left[V_{\max}\frac{\tanh(z_{i+1}+d-d_0)-\tanh(z_i+d-d_0)}{1+\tanh(d_0)} - y_i\right] \end{cases} \quad (3)$$

where $d_0 = l_v + d_s$ and, when $i = N$, $i+1 = 1$. Therefore, the uniform flow equilibrium (2) corresponds to the origin, because $z_i = z_* = \Delta x_* - d = 0$ and $y_i = y_* = 0$. Since the vehicles travel on a closed ring road, their relative distances must satisfy $\sum_{i=1}^{N}\Delta x_i = \sum_{i=1}^{N}(z_i + d) = L$. Since $L = Nd$, the sum of the spacing errors is equal to zero, which allows writing z_N as a function of the other variables. The resulting Reduced Optimal Velocity Model is

$$\begin{aligned} &\dot{z}_i = y_i, \qquad i = 1, \dots, N-1 \\ &\dot{y}_i = bV_{\max}\frac{\tanh(z_{i+1}+d-d_0)-\tanh(z_i+d-d_0)}{1+\tanh(d_0)} - by_i, \\ &\qquad\qquad \forall\ i = 1, \dots, N-2 \\ &\dot{y}_{N-1} = bV_{\max}\frac{\tanh\left(-\sum_{i=1}^{N-1} z_i + d - d_0\right)-\tanh(z_{N-1}+d-d_0)}{1+\tanh(d_0)} - by_{N-1} \\ &\dot{y}_N = bV_{\max}\frac{\tanh(z_1+d-d_0)-\tanh\left(-\sum_{i=1}^{N-1} z_i + d - d_0\right)}{1+\tanh(d_0)} - by_N \end{aligned} \quad (4)$$

The origin is an equilibrium point of model (4) and corresponds to the uniform flow equilibrium.

III. Linear analysis

With the objective of unveiling some structural properties of system (3), in this section we present some preliminary results based on a linear analysis around the zero equilibrium point. We therefore linearize the Reduced Optimal Velocity Model (4) around the origin, thereby obtaining

$$\begin{aligned} &\dot{z}_i = y_i, \quad \forall\ i = 1, \dots, N-1 \\ &\dot{y}_i = -\gamma z_i + \gamma z_{i+1} - by_i, \quad \forall\ i = 1, ..., N-2 \\ &\dot{y}_{N-1} = -\gamma \sum_{j=1}^{N-2} z_j \ - 2\gamma z_{N-1} \ - by_{N-1} \\ &\dot{y}_N = 2\gamma z_1 + \gamma \sum_{j=1}^{N-2} z_j \ - by_N \end{aligned} \quad , \quad (5)$$

where $\gamma = b\frac{\partial V_{opt}(d)}{\partial z_i} = bV_{\max}\frac{\operatorname{sech}^2(d-d_0)}{1+\tanh(d_0)}$. Using the state vector

$$\tilde{\chi} = [z_1, z_2, ..., z_{N-1}, y_1, y_2, ..., y_N]^T \in \mathbb{R}^{2N-1}, \quad (6)$$

we obtain $\dot{\tilde{\chi}} = \tilde{J}\tilde{\chi}$, where

$$\tilde{J} = \begin{bmatrix} 0 & \tilde{J}_{zy} \\ \tilde{J}_{yz} & -bI_N \end{bmatrix},$$

$$\tilde{J}_{yz} = \frac{bV_{\max}\operatorname{sech}^2(d-d_0)}{1+\tanh(d_0)}\begin{bmatrix} -1 & 1 & & (0) \\ & \ddots & \ddots & \\ (0) & & -1 & 1 \\ -1 & \dots & -1 & -2 \\ 2 & 1 & \dots & 1 \end{bmatrix} \in \mathbb{R}^{N\times N-1},$$

$$\tilde{J}_{zy} = \begin{bmatrix} 1 & & (0) & 0 \\ & 1 & & \vdots \\ & \ddots & & \vdots \\ (0) & & 1 & 0 \end{bmatrix} \in \mathbb{R}^{N-1\times N}.$$

Its stability properties are stated in the following result, which is a corollary of recent stability results by [7].

Theorem 1. *The most critical eigenvalue λ_* of the linearized reduced model (5) around the uniform flow equilibrium has real part*

$$\Re(\lambda_*) = -\frac{b}{2}+\frac{1}{2}\Big(\frac{\sqrt{b^4+32\gamma^2 a_N - 8b^2\gamma a_N}+b^2-4\gamma a_N}{2}\Big)^{\frac{1}{2}},$$

where $a_N = 1-\cos(\frac{2\pi}{N})$ and $\gamma = bV_{\max}\dfrac{\operatorname{sech}^2(d-d_0)}{1+\tanh(d_0)}$, and the uniform flow equilibrium is asymptotically stable if and only if the parameters satisfy the following constraint:

$$\frac{V_{\max}}{b}\frac{\operatorname{sech}^2(d-d_0)}{1+\tanh(d_0)} < \frac{1}{1+\cos(\frac{2\pi}{N})} =: \kappa_N. \qquad (7)$$

Proof. The characteristic polynomial of $\tilde{J}$ can be explicitly computed as:

$$\det(\tilde{J}-\lambda I) = (\lambda+b)\prod_{k=1}^{N-1}(\lambda^2+b\lambda+\gamma-\gamma e^{\frac{2k\pi j}{N}}). \qquad (8)$$

By comparing this expression with the characteristic polynomial in [7, Appendix A], we can apply the necessary and sufficient stability conditions in [7, Theorem 1]. Specializing these conditions to our model, we obtain:

$$\frac{V_{\max}}{b}\frac{\operatorname{sech}^2(d-d_0)}{1+\tanh(d_0)} < \frac{1}{1+\cos(\frac{2\pi(i-1)}{N})},\ \forall\ i=2,...,N$$

The most restrictive constraint is obtained for $i=2$, thereby leading to (7). □

The stability of the equilibrium depends on the parameters. Considering the stability condition (7), the uniform flow equilibrium may become unstable when b decreases, $V_{\max}$ increases or $|d-d_0|$ decreases. If we fix $d_0 = l_v + d_s$ and the number of vehicles, then the stability of the uniform flow equilibrium depends on the length L of the ring road. If ring road is too long ($d \gg d_0$), then the left-hand side term of (7) is very close to zero for any b and $V_{\max}$. Thus, the stability constraint is satisfied. Nevertheless, as $|d-d_0|$ increases, the most critical eigenvalue tends to the imaginary axis. In particular,

$$\lim_{|d-d_0|\to\infty}\Re(\lambda_*) = 0,$$

so the uniform flow equilibrium is asymptotically stable, but the convergence of the trajectories towards it is slow.

The stability conditions also depend on the number of vehicles N. As N increases, the stability constraint (7) becomes more restrictive, so the set of the parameters for which the uniform flow equilibrium is asymptotically stable is smaller. However, since $\kappa_N \geq 1/2$, for any N there exists a set of parameters (b, $V_{\max}$, L, d_0) such that asymptotic stability of the uniform flow equilibrium is ensured. Moreover, the size of the group of vehicles affects also $\Re(\lambda_*)$. Assume to increase N and the length L of the ring road such that $d = \frac{L}{N}$ is constant. Then,

$$\lim_{N\to\infty}\Re(\lambda_*) = 0.$$

Thus, as the number of vehicles and the length of the ring increase, convergence of the trajectories to the uniform flow equilibrium gets slower. The effect of b, $V_{\max}$, $d-d_0$, and N on the stability will be confirmed by the nonlinear analysis that is presented in the next section.

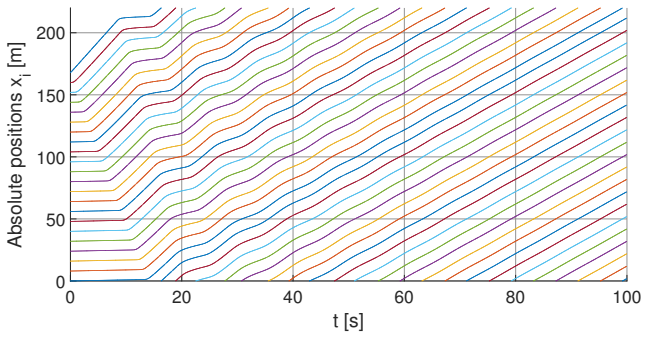

Fig. 1: Absolute positions x_i of a group of $N=22$ vehicles, with $b=10\ s^{-1}$ and $V_{\max}=5\ m/s$.

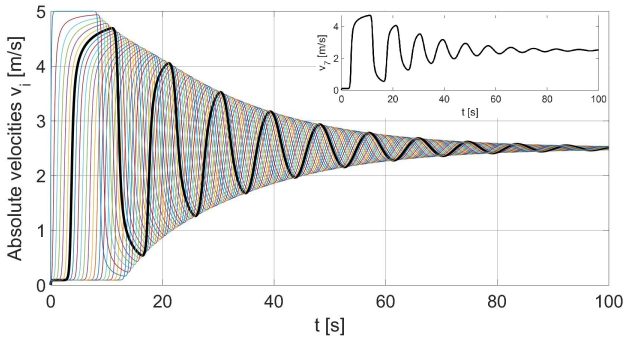

Fig. 2: Absolute velocities v_i of a group of $N=22$ vehicles, with $b=10\ s^{-1}$ and $V_{\max}=5\ m/s$.

In order to illustrate the value of the above stability analysis, we simulate the Optimal Velocity Model on a ring road and show that when the linearization is not stable, the nonlinear OVM model produces stop-and-go-waves. To this purpose, we present two simulations of a group of $N=22$ vehicles on a ring of length $L=220\ m$, where $d_0 = l_v + d_s = 10\ m$, with two different choices of b and $V_{\max}$.

Example 1 (Asymptotically stable equilibrium)**.** *If $b=10\ s^{-1}$ and $V_{\max}=5\ m/s$, then the stability condition (7) is satisfied. The trajectories of the model converge to the uniform flow equilibrium, as shown in Fig. 1 and Fig. 2.*

Example 2 (Unstable equilibrium)**.** *If $b=3\ s^{-1}$ and $V_{\max}=15\ m/s$, the stability condition (7) is not satisfied and the uniform flow equilibrium is unstable. In simulation, the trajectories of (1) produce stop-and-go waves even if they start from the uniform flow equilibrium, as shown in Fig. 3 and Fig. 4.*

IV. Nonlinear analysis: Regions of Attraction

The analysis presented in Section III enables to outline some structural conditions to ensure local asymptotic stability of (3). However, the results in Section III are based on a linearized model and therefore only apply locally and do not provide any information on the region of attraction of the origin for

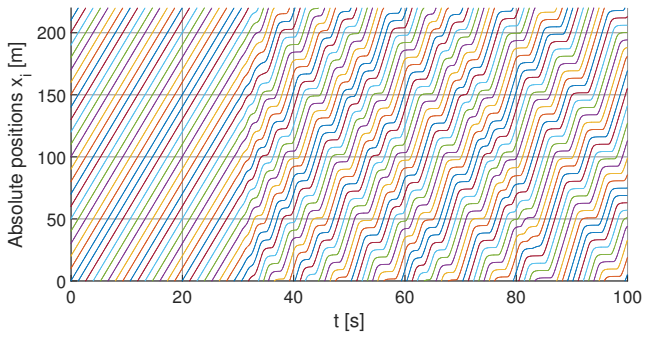

Fig. 3: Absolute positions x_i of a group of $N = 22$ vehicles, with $b = 3\ s^{-1}$ and $V_{\max} = 15\ m/s$.

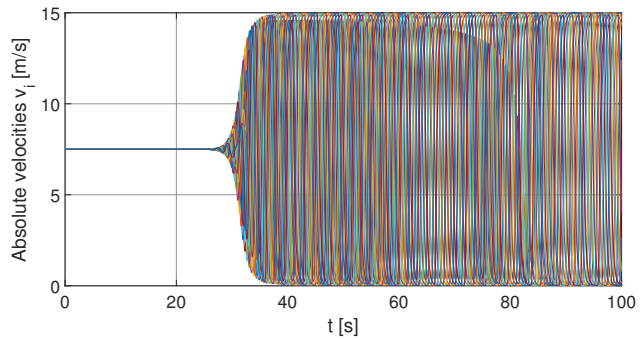

Fig. 4: Absolute velocities v_i of a group of $N = 22$ vehicles, with $b = 3\ s^{-1}$ and $V_{\max} = 15\ m/s$.

the actual dynamics, which can potentially be quite small. In this sense, the results in Section III may be difficult to exploit in practice. To overcome this drawback, in this section we focus on the nonlinear system (4) and determine an ellipsoidal inner estimate of the *region of attraction* (ROA) of the origin, which is the region of attraction of the uniform flow for the nonlinear system (1). To this end, we rely on the results in [14] to encapsulate the nonlinearity $\tanh$ into a local sector bound. This method enables to devise sufficient conditions in terms of matrix inequalities that can be efficiently exploited to obtain ellipsoidal estimates of the ROA.

System (4) can be rewritten as:

$$\dot{\tilde{\chi}} = A\tilde{\chi} + B\tanh(K\tilde{\chi} + \bar{d}), \tag{9}$$

where $\tilde{\chi}$ is defined in (6), $\bar{d} \coloneqq (d - d_0)\mathbb{1}_N$, and $A \coloneqq \begin{bmatrix} 0 & A_{zy} \\ 0 & -bI_N \end{bmatrix}$, with

$$A_{zy} \coloneqq \begin{bmatrix} 1 & & & 0 & 0 \\ & 1 & & & \vdots \\ & & \ddots & & \vdots \\ 0 & & & 1 & 0 \end{bmatrix} \in \mathbb{R}^{N-1\times N}$$

$$B \coloneqq \begin{bmatrix} 0_{N-1\times N} \\ B_{yz} \end{bmatrix} \in \mathbb{R}^{2N-1\times N}$$

where

$$B_{yz} \coloneqq \frac{bV_{\max}}{1+\tanh(d_0)} \begin{bmatrix} -1 & 1 & & & (0) \\ & -1 & 1 & & \\ & & \ddots & \ddots & \\ (0) & & & -1 & 1 \\ 1 & 0 & \dots & 0 & -1 \end{bmatrix} \in \mathbb{R}^{N\times N}$$

and $K \coloneqq \begin{bmatrix} K_{yz} & 0_{N\times N} \end{bmatrix} \in \mathbb{R}^{N\times 2N-1}$, with

$$K_{yz} \coloneqq \begin{bmatrix} 1 & & & (0) \\ & 1 & & \\ & & \ddots & \\ (0) & & & 1 \\ -1 & \dots & \dots & -1 \end{bmatrix} \in \mathbb{R}^{N\times N-1}.$$

We compute an underestimate of the ROA of the origin of (4). In particular, notice that for all $d, d_0 \in \mathbb{R}$, $B\bar{d} = 0$, thereby confirming that $\tilde{\chi} = 0$ is an equilibrium for (4). Similarly as in [14], we inscribe the nonlinearity $\tanh$ into a local sector bound by the following lemma [14, Lemma 1].

Lemma 1. *Let $\underline{\nu}$ and $\bar{\nu}$ be real numbers, $\nu_\star \in [\underline{\nu}, \bar{\nu}]$, and*

$$\alpha(\underline{\nu}, \bar{\nu}) \coloneqq \min\left\{ \frac{\tanh(\bar{\nu}) - \tanh(\nu_*)}{\bar{\nu} - \nu_*}, \frac{\tanh(\nu_*) - \tanh(\underline{\nu})}{\nu_* - \underline{\nu}} \right\}$$

where $\alpha < 1$. Then, for all $\underline{\nu} \le \nu \le \bar{\nu}$, one has that $\tanh(\nu)$ lies within the local sector $[\alpha(\underline{\nu}, \bar{\nu}), 1]$ centered in $(\nu_*, \tanh(\nu_*))$. Namely, for all $\nu \in [\underline{\nu}, \bar{\nu}]$

$$(\Delta y(\nu) - \alpha(\underline{\nu}, \bar{\nu})\Delta\nu)(\Delta\nu - \Delta y(\nu)) \ge 0, \tag{10}$$

where $\Delta y(\nu) \coloneqq \tanh(\nu) - \tanh(\nu_*)$ and $\Delta\nu \coloneqq \nu - \nu_*$. □

In the remainder of the analysis, we take $\nu_* = d - d_0$. In the particular case in which $d = d_0$, it turns out that $\bar{d} = 0$, hence $\tanh$ is inscribed in a local sector centered in the origin.

Lemma 1 can be used to obtain a sector condition for the vector valued function $\tanh\colon \mathbb{R}^N \to \mathbb{R}^N$, this is due to the decentralized nature of such a function. In particular, let $\underline{v}, \bar{v} \in \mathbb{R}^N$, $a \in \mathbb{R}^N$, where for all $i \in \{1, 2, \dots, N\}$, $a_i \coloneqq \alpha(\underline{v}_i, \bar{v}_i)$. Then, from Lemma 1, for all $\underline{v} \preceq v \preceq \bar{v}$, $\underline{v} \preceq v_* \preceq \bar{v}$

$$\zeta(v, v_*)^T \Psi^T M(\lambda) \Psi \zeta(v, v_*) \ge 0, \tag{11}$$

where

$$\zeta(v, v_*) \coloneqq \begin{bmatrix} v - v_* \\ \tanh(v) - \tanh(v_*) \end{bmatrix}, \Psi \coloneqq \begin{bmatrix} I_N & -I_N \\ -\operatorname{diag}(a) & I_N \end{bmatrix},$$

$$M(\lambda) \coloneqq \begin{bmatrix} 0_{N\times N} & \operatorname{diag}(\lambda) \\ \operatorname{diag}(\lambda) & 0_{N\times N} \end{bmatrix}, \quad \lambda \in \mathbb{R}^N_{\ge 0}.$$

Condition (11) is used to state the following result, which is a continuous-time version of [14, Theorem 1].

Theorem 2 (LMIs & Regions Of Attraction)**.** *Consider system (9). Let $v_* = \bar{d}$, $\bar{v} \succeq v_*$, and $\underline{v} = 2v_* - \bar{v}$. Define the following matrices:*

$$R \coloneqq \begin{bmatrix} I_n & 0_{n\times N} \\ 0_{N\times n} & I_N \end{bmatrix}, Q \coloneqq \begin{bmatrix} K & 0_{N\times N} \\ 0_{N\times n} & I_N \end{bmatrix},$$

where $n \coloneqq 2N - 1$. If there exist a symmetric positive definite matrix $P \in \mathbb{R}^{n\times n}$ and a vector $\lambda \in \mathbb{R}^N_{\ge 0}$ such that

$$R^T \begin{bmatrix} A^TP - PA & PB \\ B^TP & 0 \end{bmatrix} R + Q^T\Psi^T M(\lambda)\Psi Q < 0 \tag{12}$$

$$\begin{bmatrix} (\bar{v}_{(i)} - v_{*_{(i)}})^2 & K_{(i)} \\ K_{(i)}^T & P \end{bmatrix} \geq 0,\ i = 1, \dots, N, \tag{13}$$

where $K_{(i)}$ is the i-th line of K, $K_{(i)}^T$ is its transpose, $v_{*_{(i)}}$ and $\bar{v}_{(i)}$ are the i-th elements of v_* and $\bar{v}$ respectively. Then

$$\mathcal{E}(P) \coloneqq \{\tilde{\chi} \in \mathbb{R}^n :\ \tilde{\chi}^T P \tilde{\chi} \leq 1\}$$

is forward invariant and included in the ROA of the origin of system (9).

Proof. The satisfaction of (13) guarantees that

$$\mathcal{E}(P) \subseteq \{\tilde{\chi} \in \mathbb{R}^n :\ \underline{v} - v_* \preccurlyeq K\tilde{\chi} \preccurlyeq \bar{v} - v_*\},$$

In particular, for all $\tilde{\chi} \in \mathcal{E}(P)$, (11) holds. Let us consider the following quadratic Lyapunov function candidate $V(\tilde{\chi}) \coloneqq \tilde{\chi}^T P \tilde{\chi}$. To prove the result, we show that for all $\tilde{\chi} \in (\mathcal{E}(P) \setminus \{0\})$

$$\dot{V}(\tilde{\chi}) = \dot{\tilde{\chi}}^T P \tilde{\chi} + \tilde{\chi}^T P \dot{\tilde{\chi}} < 0. \tag{14}$$

The latter can be written in the following matrix form:

$$\dot{V}(\tilde{\chi}) = \begin{bmatrix} \tilde{\chi}^T & (u - u_*)^T \end{bmatrix} \begin{bmatrix} A^T P + PA & PB \\ B^T P & 0 \end{bmatrix} \begin{bmatrix} \tilde{\chi} \\ u - u_* \end{bmatrix}. \tag{15}$$

where we use the shorthand notation $u = \tanh(K\tilde{\chi} + \overline{d})$ and $u_* = \tanh(\overline{d})$.

By pre-and-post multiplying the matrix in the lefthand side of (12) by $[\tilde{\chi}^T\ (u - u_*)^T]$ and its transpose, one gets:

$$W(\tilde{\chi}) \coloneqq \begin{bmatrix} \tilde{\chi}^T & (u - u_*)^T \end{bmatrix} \begin{bmatrix} A^T P + PA & PB \\ B^T P & 0 \end{bmatrix} \begin{bmatrix} \tilde{\chi} \\ u - u_* \end{bmatrix} + \begin{bmatrix} v - v_* \\ u - u_* \end{bmatrix}^T \Psi^T M(\lambda) \Psi \begin{bmatrix} v - v_* \\ u - u_* \end{bmatrix}.$$

Therefore, by using (12) and (15), it follows that

$$W(\tilde{\chi}) = \dot{V}(\tilde{\chi}) + \begin{bmatrix} v - v_* \\ u - u_* \end{bmatrix}^T \Psi^T M(\lambda) \Psi \begin{bmatrix} v - v_* \\ u - u_* \end{bmatrix} < 0.$$

The latter with (11) yields (14) and concludes the proof. □

Theorem 2 enables to obtain an ellipsoid that is an inner-approximation of the ROA of model (4). With the objective of reducing the conservatism in the estimation of the ROA, we embed the conditions of Theorem 2 into a suitable optimization problem aimed at maximizing the size of the ellipsoidal set $\mathcal{E}(P)$. To this end, a possible approach consists of minimizing the trace of matrix P. Specifically, an optimal estimate of the ROA can be obtained by solving the following optimization problem:

$$\begin{aligned} &\text{minimize} && \operatorname{trace}(P) \\ &\text{subject to} && \text{inequalities } (12), (13). \end{aligned} \tag{16}$$

When $\bar{v}$ is fixed, conditions (12) (13) are linear matrix inequalities in the decision variables P and λ. Therefore, (16) can be efficiently solved via off-the-shelf software, with the only caveat of selecting the vector $\bar{v}$. Notice that since $\mathcal{E}(P)$ is contained in the polyhedral set $\{\tilde{\chi} \in \mathbb{R}^n :\ \underline{v} - v_* \preccurlyeq K\tilde{\chi} \preccurlyeq \bar{v} - v_*\}$, the selection of the values of $\bar{v}$ affects the size of the ellipsoidal estimate in several ways. In particular, the larger is $\bar{v}$, the wider is the local sector and the volume of the ellipsoid. Nevertheless, increasing too much $\bar{v}$ may lead to no feasible solutions for problem (16). For this reason, the choice of $\bar{v}$ requires a trade-off between the quality of the approximation and the feasibility of the optimization problem. As in Example 3, given the model parameters, the best estimate is obtained with the maximum $\bar{v}$ for which the optimization problem is feasible.

TABLE I: Dependence of the ellipsoidal estimate on b. Increasing b, the levels $\bar{v}$ increases and the size of $\mathcal{E}(P)$ increases. $V_{\max} = 5\ m/s$ and $d = d_0$.

$b\ [s^{-1}]$	Vector $\bar{v}$	Volume of $\mathcal{E}(P)$	z_1 and $y_1 \in \mathcal{E}(P)$
$b = 10$	$\bar{v}_{(i)} = 0.7089$	1.31×10^4	$\lvert z_1\rvert \leq 0.7088\ m$ $\lvert y_1\rvert \leq 4.02\ m/s$
$b = 20$	$\bar{v}_{(i)} = 0.8750$	2.20×10^{11}	$\lvert z_1\rvert \leq 0.8750\ m$ $\lvert y_1\rvert \leq 6.77\ m/s$
$b = 30$	$\bar{v}_{(i)} = 0.9143$	1.37×10^{14}	$\lvert z_1\rvert \leq 0.9141\ m$ $\lvert y_1\rvert \leq 8.74\ m/s$

Example 3 (Ellipsoidal ROA)**.** *We consider a platoon of $N = 22$ vehicles. Consider the same parameters of Example 1, where $b = 10\ s^{-1}$, $V_{\max} = 5\ m/s$ and $d_0 = 10\ m$. Thus, the stability constraint (7) is satisfied and the origin is an asymptotically stable equilibrium point for the model. Assume the length L of the ring road is such that $d = \frac{L}{N}$ equals $d_0 = l_v + d_s = 10\ m$, then $v_* = u_* = 0$. The maximum value of $\bar{v}_{(i)}$ for which (16) is feasible is $\bar{v}_{(i)} = 0.7089,\ \forall\ i = 1, 2, \dots, N$. We compute the maximum-volume ellipsoid $\mathcal{E}(P) \in \mathbb{R}^{43}$ and in Figure 5 are shown its intersections with (z_1, z_2) and (y_1, y_2) planes.*

The parameters of the model affect the maximum value of $\bar{v}$ for which (16) is feasible, so they ultimately affect the size of the maximum-volume ellipsoidal estimate. Moreover, the dependence on the parameters of the volume of the best approximation of the ROA of the nonlinear model (4) around the origin reflects the relationship between the parameters and the eigenvalues of the linearized model (5) around the origin.

If $d - d_0 \neq 0$, then $v_*, u_* \neq 0$ and the local sectors are not centered at the origin: in this case the choice of $\bar{v}$ is limited to small values with respect to v_* and the volume of the resulting ellipsoidal estimate is small. On the contrary, if $d = d_0$ the local sectors are centered in the origin and we get the largest ellipsoidal estimate. Also the number of vehicles affects the size of the maximum-volume ellipsoidal estimate of the ROA. In particular, as N increases, the maximum value of $\bar{v}$ for which the optimization problem (16) is feasible decreases, leading to ellipsoids with smaller volume. Finally, we analyze the dependence of the size of the ellipsoidal estimate of the ROA of the nonlinear model (4) around the origin on b and $V_{\max}$. We fix $d = d_0$, compute the ellipsoidal estimates for different values of b and $V_{\max}$ and see that reducing b and increasing $V_{\max}$ lead to smaller maximum values of $\bar{v}_{(i)}$ for which problem (16) is feasible and to smaller ellipsoidal estimates. Let us fix $V_{\max} = 5\ m/s$, compute $\mathcal{E}(P)$ for different values of b and project it on subspaces generated by bases of the state variables. In Table I are shown the ranges of the state variables belonging to $\mathcal{E}(P)$ and the corresponding volumes. As expected, by increasing b, the volume of the ellipsoidal estimate of the ROA increases. The

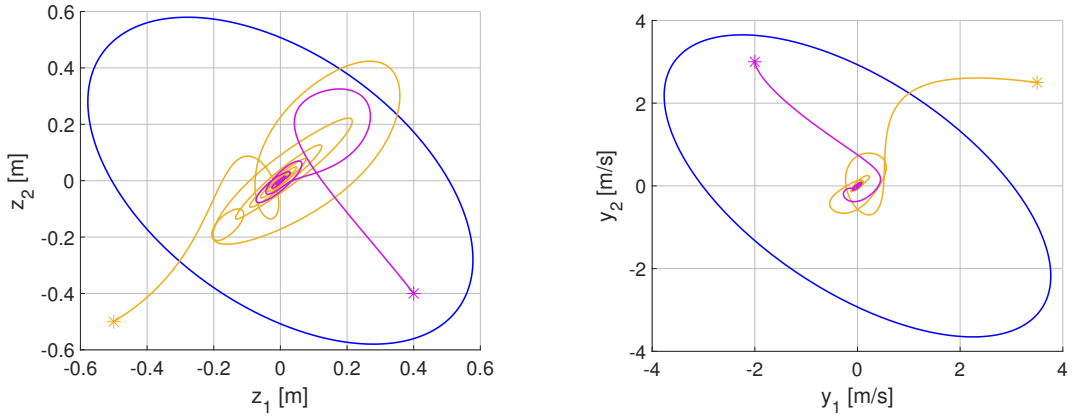

Fig. 5: Example 3 - Cross-sections of $\mathcal{E}(P)$ (blue) in the (z_1, z_2) plane (left) and in the (y_1, y_2) plane (right), together with illustrative trajectories (whose starting points are marked by a star). The purple trajectory starts inside $\mathcal{E}(P)$, remains inside by invariance and converges to the origin. Being $\mathcal{E}(P)$ an underestimate of the ROA, there are trajectories (like the orange one) that converge to the origin even if they originate from outside the ellipsoid.

TABLE II: Dependence of the ellipsoidal estimate on $V_{\max}$. Increasing $V_{\max}$, the levels $\bar{v}$ decrease and the size of $\mathcal{E}(P)$ decreases. $b = 20\ s^{-1}$ and $d = d_0$.

$V_{\max}\ \left[\frac{m}{s}\right]$	Vector $\bar{v}$	Volume of $\mathcal{E}(P)$	z_1 and $y_1 \in \mathcal{E}(P)$
$V_{\max} = 5$	$\bar{v}_{(i)} = 0.8750$	2.20×10^{11}	$\lvert z_1\rvert \leq 0.8750\ m$ $\lvert y_1\rvert \leq 6.77\ m/s$
$V_{\max} = 10$	$\bar{v}_{(i)} = 0.7171$	2.13×10^{6}	$\lvert z_1\rvert \leq 0.7171\ m$ $\lvert y_1\rvert \leq 7.57\ m/s$
$V_{\max} = 15$	$\bar{v}_{(i)} = 0.5109$	117.03	$\lvert z_1\rvert \leq 0.5108\ m$ $\lvert y_1\rvert \leq 6.62\ m/s$

ellipsoids are inner-approximations, so we can't state whether tuning b actually makes the ROA enlarge, but a larger b allows to get to a wider set of initial conditions for which we are sure the trajectories of (4) converge to the uniform flow equilibrium. Finally, we compute the ellipsoidal estimates by solving (16) fixing $b = 20\ s^{-1}$ with different values of $V_{\max}$. The ellipsoids are projected on subspaces generated by bases of the state variables. In Table II are shown the ranges of the state variables belonging to $\mathcal{E}(P)$ and the corresponding volumes. By increasing $V_{\max}$, the volume of the ellipsoidal estimates of the ROA decreases, meaning that the set of initial conditions, from which the trajectories of (4) converge to the uniform flow equilibrium, becomes smaller.

V. Invariance-based Safety Analysis

Besides the convergence of the trajectories of model (1) to the uniform flow equilibrium, we are interested in vehicle safety. To this goal, maintaining the inter-vehicle distances above a certain minimum value is beneficial in order to avoid collisions. Let us suppose that the minimum safe inter-vehicle distance would be $d_{\min} = 8\ m$. In Fig. 6 are shown the relative distances of the time simulation of a group of 22 vehicles on a ring of length $L = 220\ m$. The parameters of the model do not satisfy the stability condition and the vehicles do not keep the minimum distance $d_{\min}$.

The method put in place in Section IV to determine invariant ellipsoidal sets is suitable to include safety constraints to

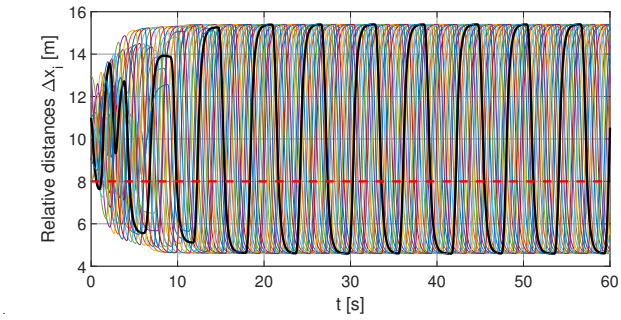

Fig. 6: Evolution of the vehicle distances with respect to time. The distance between the 21^{st} and the 20^{th} vehicle is in bold black. With $b = 3\ s^{-1}$, $V_{\max} = 20\ m/s$ and $d = d_0$, the distances are not safe, as they reach values lower than $d_{\min} = 8\ m$.

avoid accidents. To prevent the collision between two adjacent vehicles, we can impose a lower bound on their distance Δx_i or, equivalently, on their spacing error $z_i = \Delta x_i - d$. Let us consider the following constraints on the minimum and the maximum inter-vehicle distances Δx_i:

$$d_{\min} \leq \Delta x_i \leq d_{\max}, \tag{17}$$

where $d_{\min}$ is the safety distance and $d_{\max}$ is the maximum allowed inter-vehicle distance. Condition (17) can be obtained by imposing the following constraints on the spacing errors $z_i, \forall\ i = 1, \ldots, N-1$:

$$d_{\min} - d \leq z_i \leq d_{\max} - d, \tag{18}$$

where $d = L/N$. These constraints are encoded in a symmetric polytope defined as

$$S(|Q|, \rho) := \{\tilde{\chi} \in \mathbb{R}^n :\ |Q\tilde{\chi}| \preceq \rho\}, \tag{19}$$

where $\tilde{\chi}$ is the state vector (6), the safety ranges are defined in (18), where $d_{\min} - d = -(d_{\max} - d)$ to get a symmetric polytope, $Q = \begin{bmatrix} I_{N-1} & 0_{N-1\times N} \end{bmatrix} \in \mathbb{R}^{N-1\times 2N-1}$, with I_{N-1} the

identity matrix $\in \mathbb{R}^{N-1\times N-1}$, and $\rho = (d_{\max} - d)\mathbb{1} \in \mathbb{R}^{N-1}$. The objective is then to find the maximum-volume ellipsoidal estimate of the ROA for system (4) that lies inside the safety polytope $S(|Q|, \rho)$. In this way, by starting the trajectories inside the resulting ellipsoid, not only the vehicles reach the uniform flow equilibrium, but they will travel at safe distance.

It is shown in [15, Appendix C.8.3] that the ellipsoid $\mathcal{E}(P) = \{\tilde{\chi} \in \mathbb{R}^n \colon \tilde{\chi}^T P \tilde{\chi} \leq 1\}$ can be included in a symmetric polytope $S(|Q|, \rho)$, with $Q \in \mathbb{R}^{m\times n}$ by enforcing the following inequality for each element of vector ρ:

$$\begin{bmatrix} P & Q_{(i)}^T \\ Q(i) & \rho_{(i)}^2 \end{bmatrix} \geq 0, \quad \forall i \in \{1, 2, \ldots, m\} \tag{20}$$

where $Q_{(i)}^T$ is the transpose of the i-th row of Q. To find an ellipsoid included into the intersection of the ROA and a safety symmetric polytope $S(|Q|, \rho)$, one can include (20) in the set of constraints of the optimization problem (16). The resulting optimization problem is then

$$\begin{aligned} &\text{minimize} \quad \text{trace}(P) \\ &\text{subject to} \quad \text{inequalities } (12), (13), (20). \end{aligned} \tag{21}$$

Being $\mathcal{E}(P)$ an invariant and contractive set, if the trajectories of system (4) are initialized inside it, they remain within this set and converge to the origin. Therefore, the vehicles keep a minimum inter-vehicle distance $d_{\min}$.

In the following example, we compute the maximum-volume ellipsoidal estimate of the ROA included in a safety polytope for the model (4). The estimate of the ROA provided by the solution of (16) is not safe, therefore, solving problem (21) provides a smaller ellipsoid that guarantees the safety of the trajectories.

Example 4. *Consider a group of $N = 5$ vehicles that travel on a ring of length $L = 50$ m. Assume the model parameters are $b = 20$ s^{-1}, $V_{\max} = 5$ m/s and $d_0 = 10$ m. The maximum-volume ellipsoidal estimate of the ROA is obtained for $\bar{v}_{(i)} = 3.1308$ and its cross-section in the (z_1, z_2) plane is shown in Fig. 7 in blue. Suppose to force the constraint on the vehicle distances,*

$$8 \ m \leq \Delta x_i \leq 12 \ m, \tag{22}$$

then the ellipsoid should lie in a safety polytope $S(|Q|, \rho)$ where $\rho = 2$ m. Since our ellipsoidal estimate is not included in the polytope, we add (20) and find a smaller ellipsoid whose section on (z_1, z_2) is shown in Figure 7 in red. The trajectories that start inside this smaller ellipsoid converge to the origin and the vehicle distances satisfy the safety constraints (22).

VI. Conclusion

The stability of the Optimal Velocity model has been investigated by completing the local linearization-based analysis with a more refined nonlinear analysis. Sufficient conditions based on LMIs have been proposed to determine ellipsoidal estimates of the region of attraction of the nonlinear model. The relationship between stability of the uniform flow equilibrium and the model parameters is first probed by the linearized model and then confirmed by the analysis in the nonlinear framework. In the linear model, some choices of the parameters may lead to eigenvalues with positive real part and make the uniform flow an unstable equilibrium. In the nonlinear context, the same behaviour of the parameters leads to smaller ellipsoidal estimates of the region of attraction. The nonlinear analysis also brings a contribution regarding safety: the computation of invariant and contractive sets for the uniform flow equilibrium allows us to identify sets of initial conditions such that the trajectories of a group of N vehicles do not collide.

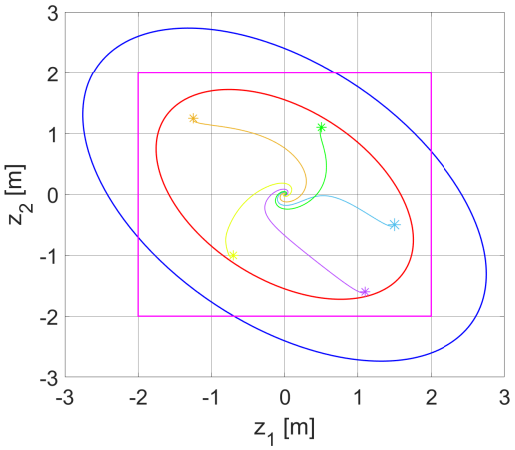

Fig. 7: Example 4 - Cross-sections in the (z_1, z_2) plane of the maximum-volume estimate of the ROA (blue), the safety polytope $S(|Q|, \rho)$ (pink), and the ellipsoidal estimate included in the safety polytope (red). The trajectories initialized inside the invariant safe ellipsoid (red) stay within it.

A possible improvement of the nonlinear analysis is to use non-quadratic Lyapunov function and get polytopic estimates of the region of attraction instead of ellipsoids. The polytopic representation can potentially provide a clearer view of the set of initial conditions from which the trajectories converge to the equilibrium. Future work should also focus on the introduction of a control input on one of the vehicles in order to improve stability, enlarge the basin of attraction of the uniform flow equilibrium, and avoid instability and collisions. The presence of an input represents the action of an AV and the analysis would help to understand the interconnection between AVs and human-driven vehicles.

References

[1] Y. Sugiyama, M. Fukui, M. Kikuchi, K. Hasebe, A. Nakayama, K. Nishinari, S. ichi Tadaki, and S. Yukawa, "Traffic jams without bottlenecks—experimental evidence for the physical mechanism of the formation of a jam," *New Journal of Physics*, vol. 10, no. 3, p. 033001, 2008.

[2] R. E. Stern, S. Cui, M. L. Delle Monache, R. Bhadani, M. Bunting, M. Churchill, N. Hamilton, R. Haulcy, H. Pohlmann, F. Wu, B. Piccoli, B. Seibold, J. Sprinkle, and D. B. Work, "Dissipation of stop-and-go waves via control of autonomous vehicles: Field experiments," *Transportation Research Part C: Emerging Technologies*, vol. 89, pp. 205–221, 2018.

[3] I. Gasser, G. Sirito, and B. Werner, "Bifurcation analysis of a class of 'car following' traffic models," *Physica D: Nonlinear Phenomena*, vol. 197, no. 3, pp. 222–241, 2004.

[4] S. Feng, Y. Zhang, S. E. Li, Z. Cao, H. X. Liu, and L. Li, "String stability for vehicular platoon control: Definitions and analysis methods," *Annual Reviews in Control*, vol. 47, pp. 81–97, 2019.

[5] R. Merco, F. Ferrante, and P. Pisu, "A hybrid controller for DoS-resilient string-stable vehicle platoons," *IEEE Transactions on Intelligent Transportation Systems*, vol. 22, no. 3, pp. 1697–1707, 2021.

[6] C. Wu, A. M. Bayen, and A. Mehta, "Stabilizing traffic with autonomous vehicles," in *2018 IEEE International Conference on Robotics and Automation (ICRA)*, pp. 6012–6018, 2018.

[7] V. Giammarino, S. Baldi, P. Frasca, and M. L. Delle Monache, "Traffic flow on a ring with a single autonomous vehicle: An interconnected stability perspective," *IEEE Transactions on Intelligent Transportation Systems*, vol. 22, no. 8, pp. 4998–5008, 2021.

[8] Y. Zheng, J. Wang, and K. Li, "Smoothing traffic flow via control of autonomous vehicles," *IEEE Internet of Things Journal*, vol. 7, no. 5, pp. 3882–3896, 2020.

[9] J. Wang, Y. Zheng, Q. Xu, J. Wang, and K. Li, "Controllability analysis and optimal controller synthesis of mixed traffic systems," in *2019 IEEE Intelligent Vehicles Symposium (IV)*, pp. 1041–1047, 2019.

[10] M. L. Delle Monache, T. Liard, A. Rat, R. Stern, R. Bhadani, B. Seibold, J. Sprinkle, D. B. Work, and B. Piccoli, *Feedback Control Algorithms for the Dissipation of Traffic Waves with Autonomous Vehicles*, pp. 275–299. Cham: Springer International Publishing, 2019.

[11] G. Orosz and G. Stépán, "Subcritical Hopf bifurcations in a car-following model with reaction-time delay," *Proceedings of the Royal Society A: Mathematical, Physical and Engineering Sciences*, vol. 462, no. 2073, pp. 2643–2670, 2006.

[12] S. S. Avedisov and G. Orosz, "Nonlinear network modes in cyclic systems with applications to connected vehicles," *Journal of Nonlinear Science*, vol. 25, no. 4, pp. 1015–1049, 2015.

[13] M. Bando, K. Hasebe, A. Nakayama, A. Shibata, and Y. Sugiyama, "Dynamical model of traffic congestion and numerical simulation," *Phys. Rev. E*, vol. 51, pp. 1035–1042, Feb 1995.

[14] H. Yin, P. Seiler, and M. Arcak, "Stability analysis using quadratic constraints for systems with neural network controllers," *IEEE Transactions on Automatic Control*, vol. 67, no. 4, pp. 1980–1987, 2022.

[15] S. Tarbouriech, G. Garcia, J. M. Gomes da Silva Jr, and I. Queinnec, *Stability and Stabilization of Linear Systems with Saturating Actuators*. Springer, 2011.

Francesco Ferrante (STM'11-M'16-SM'22) received the B.Sc. (Laurea) degree in control engineering from the Sapienza Università di Roma, Italy, in 2010, the M.Sc. (Laurea Magistrale) degree in control engineering from the Università degli Studi di Roma Tor Vergata, Italy in 2012, and the Ph.D. degree in control theory from the Institut supérieur de l'aéronautique et de l'espace (SUPAERO) Toulouse, France, in 2015. In 2014, he held a Visiting Scholar position at the Department of Computer Engineering, University of California Santa Cruz. From November 2015 to August 2016, he was a Post-Doctoral Fellow at the Department of Electrical and Computer Engineering, Clemson University, Clemson, SC, USA. From August 2016 to September 2017, he held a position as a Post-Doctoral Scientist at the Hybrid Systems Laboratory, University of California at Santa Cruz. From September 2017 to September 2021, he was an Assistant Professor with the Faculty of Sciences, Université Grenoble Alpes, France. He also held an Adjunct Assistant Professor position at the Department of Automotive Engineering, Clemson University. Currently, he is a tenure-track assistant professor at the Department of Engineering, University of Perugia, Italy. He currently serves as an Associate Editor for the IEEE Control Systems Letters, the European Journal of Control, and IMA Journal of Mathematical Control and Information. He is a member of the conference editorial board of the European Control Association.

Cristina Magnetti Gisolo received the B.Sc. degree in Electronic Engineering, and the M.Sc. degree in Mechatronic Engineering from Politecnico di Torino, Turin, Italy, in 2018 and 2021, respectively. From September 2020 to February 2021, she was a research intern at GIPSA-lab, Grenoble, France.

Paolo Frasca (M'13–SM'18) received the Ph.D. degree from Politecnico di Torino, Turin, Italy, in 2009. After Postdoctoral appointments in Rome and in Turin, he has been an Assistant Professor with the University of Twente, Enschede, The Netherlands, from 2013 to 2016. Since October 2016, he has been CNRS Researcher with GIPSA-lab, Grenoble, France. His research interests cover the theory of control systems and networks, with main applications in infrastructural and social networks. On these topics, he has (co)authored more than fifty journal publications and the book Introduction to Averaging Dynamics Over Networks (Springer). He has been an Associate Editor for several conferences and journals, including the International Journal of Robust and Nonlinear Control, the IEEE Control Systems Letters, the Asian Journal of Control, and Automatica.

Maria Laura Delle Monache (AM'16 - M'21) is an assistant professor in the Department of Civil and Environmental Engineering and the Institute of Transportation Studies at the University of California, Berkeley. Prior to joining the faculty at UC Berkeley she was a research scientist at Inria in Grenoble, France (2016-2021) and a Postdoctoral fellow at Rutgers University - Camden in USA (2014-2016). She received the B.Sc. degree and M.Sc. degree from the university of L'Aquila (Italy), in 2009 and 2011, respectively. In 2014, she obtained the Ph.D. degree in applied mathematics from the University of Nice-Sophia Antipolis, France.